Interfacial Structure of Wild-Type and Mutant Forms of Puroindoline-b Bound to DPPG Monolayers

Luke A. Clifton,[†] Rebecca J. Green,*[,†] Arwel V. Hughes,[‡] and Richard A. Frazier[†]

Reading School of Pharmacy and Department of Food Biosciences, University of Reading, P.O. Box 226, Whiteknights, Reading RG6 6AP, United Kingdom, and ISIS Pulsed Neutron and Muon Source, Science and Technology Facilities Council Rutherford Appleton Laboratory, Harwell Science and Innovation Campus, Didcot, Oxfordshire OX11 0QX, United Kingdom

Received: July 8, 2008; Revised Manuscript Received: October 2, 2008

The interaction of wild-type puroindoline-b (Pin-b+) and two mutant forms having single residue substitutions (G46S or W44R) with L-α-dipalmitoylphosphatidyl-*dl*-glycerol (DPPG) as a Langmuir monolayer at the air/water interface was investigated by neutron reflectivity (NR) and Brewster angle microscopy (BAM). NR profiles were fitted using a three-layer model to enable differences in penetration of protein between the lipid headgroup and acyl regions to be determined. The data showed similar surface excesses for each of the three proteins at the interface; however, it was revealed that the depth of penetration of protein into the lipid region differed for each protein with Pin-b+ penetrating further into the acyl region of the lipid compared to the mutant forms of the protein that interacted with the headgroup region only. BAM images revealed that the domain structure of the DPPG monolayers was disrupted when Pin-b+ adsorption had reached equilibrium, suggesting protein penetration had led to compression of the lipid region. In contrast, the domain structure was unaffected by the W44R mutant, suggesting no change in compression of the lipid region and hence little or no penetration of protein into the lipid layer.

Introduction

The puroindolines are basic, cysteine-rich, low molecular weight proteins that occur in the seed endosperm of wheat (var. *Triticum aestivum*) as two isoforms, puroindoline-a (Pin-a) and puroindoline-b (Pin-b).[1,2] Pin-a and Pin-b exhibit approximately 55% sequence homology and lipid binding properties that are attributed to unique tryptophan-rich domains (WRWWKWWK in Pin-a and WPTKWWK in Pin-b).[3−5] In both isoforms, this tryptophan-rich domain occurs within a structural loop enclosed by a disulfide bond. The puroindolines have attracted particular attention for their role in determining wheat endosperm texture[5−7] and for their antimicrobial and antifungal activity that could be important to seed defense.[8−10] In both cases, the biochemical mechanism can be related to the lipid binding characteristics of the puroindolines.

In hexaploid wheat varieties, the gene coding of the puroindolines is linked to the *Hardness* locus (*Ha*) on the short arm of chromosome 5D, which has been shown to control endosperm texture.[11,12] The texture of the endosperm is fundamental to the milling quality of wheat and defines its end use. The wheat wild-type is soft textured, and hard wheat varieties contain either null forms or mutated forms of the genes controlling the expression of the puroindolines. This was first reported by Giroux and Morris[13] who discovered a G46S point mutation on the Pin-b gene (*Pinb-D1b*) of several hard varieties, which occurred within the tryptophan-rich loop (enclosed by a disulfide bond between C29 and C48). Further altered alleles of Pin-b were later reported, including the W44R point mutation, also within the tryptophan-rich loop.[14,15]

Our previous studies have determined that single residue substitutions in Pin-b (either G46S or W44R) lead to significant differences to the Pin-b wild-type in lipid binding behavior, which appear to correlate to the influence of these proteins on wheat endosperm texture.[16,17] In addition, the mutant forms of Pin-b exhibited lipid binding that was less selective between zwitterionic and anionic phospholipids, which could have potential impact on antimicrobial and antifungal behavior. On the basis of surface pressure and external relectance Fourier transform infrared spectroscopy data, the differences between the binding of the Pin-b mutants to monolayers of the anionic phosopholipid L-α-dipalmitoylphosphatidyl-*dl*-glycerol (DPPG) are thought to be related to the extent of penetration of the proteins into the acyl chain region of the monolayer. To test this hypothesis, the work presented here investigates the equilibrium structure of Pin-b wild-type (Pin-b+), Pin-bH (G46S substitution), and Pin-bS (W44R substitution) adsorbed to condensed phase DPPG monolayers and establishes the interfacial layer structure and the influence of the different Pin-b mutants on the domain structure of DPPG monolayers.

This work brings together the two techniques of neutron reflectivity (NR) and Brewster angle microscopy (BAM). NR has previously been employed to study the adsorption of proteins and peptides to lipid monolayers at the air/water interface[18] and is able (by suitable use of different isotopic contrasts[19]) to give information on the position of the protein at the surface with respect to the lipid monolayer. BAM has been previously used to monitor changes in the structure of lipid monolayers upon protein adsorption,[20] and its high sensitivity to density changes at the interface[21] enables changes in both the thickness and domain structures of interfacial films present at the air/water interface to be investigated.

* To whom correspondence should be addressed. E-mail: rebecca.green@reading.ac.uk. Tel: +44 118 3788446. Fax: +44 118 3784703.
[†] University of Reading.
[‡] Rutherford Appleton Laboratory.

10.1021/jp806016h CCC: $40.75
Published on Web 11/17/2008

Materials and Methods

Materials. DPPG (synthetic purity >99%) was purchased from Avanti Polar Lipids (Alabaster, AL) and used without further purification. Stock solutions (1 g dm^{-3}) of DPPG were prepared in HPLC grade chloroform (Sigma-Aldrich, Dorset, UK) and stored at room temperature with 1:2 dilutions of these solutions being used experimentally. Pin-b proteins were extracted from wheat flour and purified using Triton X-114 phase partitioning and chromatographic techniques as described previously.[16,17] All other chemicals were sourced from Sigma-Aldrich and were of the highest purity available.

Neutron Reflectivity. NR measurements were carried out using the white beam SURF reflectometer at the Rutherford Appleton Laboratory, using neutron wavelengths from 0.5 to 6.5 Å. Specular neutron reflectivity is largely determined by the variation in the scattering length density (SLD) along the surface normal.[22] As neutron scattering is a nuclear effect, different isotopes have differing scattering lengths; this allows isotopic substitution to be used to produce a number of reflectivity profiles, corresponding to a single number density profile. This provides a means of determining the composition of multicomponent systems, as shown here with the protein−lipid systems. Details of the procedures used to obtain and fit protein−lipid profiles are described in a series of previous publications.[18,19,23,24]

Protein adsorption to lipid monolayers was carried out on a polytetrafluoroethylene Langmuir trough (model 302m, Nima Technology Ltd., Coventry, U.K.) with all lipid monolayers prepared as described by Lad et al.[18] Lipid monomolecular layers were compressed and held in a condensed phase at 22 mN m^{-1} before protein solution was added. After addition of the puroindoline solutions to the subphase (final protein concentration = 0.48 μmol), neutrons were used to monitor the system until the reflectivity profile was constant and the system had therefore reached equilibrium. A reflectivity profile was then recorded at equilibrium; the collimated neutron beam was reflected at the air/liquid interface at two different glancing angles of incidence (1.5 and 0.5°). The beam intensity was calibrated with respect to a clean D_2O surface. A flat background was determined by extrapolation to high values of momentum transfer, κ ($\kappa = (4\pi \sin\theta)/\lambda$) where λ is wavelength and θ is the incident angle).

Lipid monolayers were prepared with surface pressure used to monitor film compression and NR profiles were obtained for equilibrium systems prior to and after addition of protein to the solution subphase. The subphase was composed of non-reflective water (NRW: 8% D_2O, 92% H_2O) in all experiments; this was used to make the reflectivity profile sensitive to the interfacial region only.[25] Reflectivity curves were repeated using lipids with either hydrogenated or deuterated acyl chain regions to provide isotropic contrast between the proteins and the lipids at the interface. The reflectivity profiles were analyzed using optical matrix formalism, which has been described in detail by Born and Wolf.[26]

The typical modeling procedure calculates the reflectivity profile based on fitting to the structural parameters such as number of layers at the surface, layer thickness, and SLD of each layer. Profiles measured under differing isotopic conditions are fitted to the same layer and thickness model with the SLD varying, depending on the density and composition of the protein−lipid interface. The fitted SLD for each contrast, $\rho_{(h)}$ or $\rho_{(d)}$, can be related to the volume fraction of each component in the system by

$$\rho_{(h)} = \rho_{(h-lipid)}\phi_{(h-lipid)} + \rho_{(protein)}\phi_{(protein)} + \rho_{(water)}\phi_{(water)} \quad (1)$$

$$\rho_{(d)} = \rho_{(d-lipid)}\phi_{(d-lipid)} + \rho_{(protein)}\phi_{(protein)} + \rho_{(water)}\phi_{(water)} \quad (2)$$

ϕ is the volume fraction, and ρ is the scattering length density with these values calculated for the lipid (hydrogenated (h-lipid) and deuterated (d-lipid)), protein, and water, individually. The SLD values for the lipid and protein components are shown in Table 1. The SLD values were calculated using the scattering length values quoted in Table 1 and molecular volume data calculated for lipid components as described by Lad et al.[18] The molecular volume was calculated to be 15 838 $Å^3$ for Pin-b+. Pin-bH and Pin-bS were analyzed using the scattering length (Σb), SLD (ρ), and molecular weight calculated for Pin-b+.

In the experiments described here, NRW is used, hence $\rho_{(water)}\phi_{(water)} = 0$, and is thus eliminated from the calculations. The volume fraction of both the lipid and protein can be determined from equations 1 and 2 and these used to calculate the area per molecule (A) and surface excess (Γ) of each species using[27]

$$A = \frac{\Sigma b}{\tau \phi \rho} \quad \text{and} \quad \Gamma = \frac{MW}{A6.02} \quad (3)$$

with b being the scattering length and τ the layer thickness (obtained from the model fit). The SLDs of the puroindolines were calculated assuming that 8% of the labile hydrogens on the proteins are exchanged in the NRW solution.

For the three-layer model fitting of the NR profiles, the lipid head and tail groups of the DPPG in the lipid monolayer are treated as separate layers. When describing the head and tail groups of the lipid within the monolayer as separate layers, two assumptions were made. The first assumption was that in terms of lipid component the first layer contained the lipid tail component only, while the second layer contained lipid headgroup only; the second assumption was that the area per molecule of the lipid headgroup is the same as that of the lipid acyl chain region (first layer). These assumptions were required as there was no isotopic contrast between the lipid headgroup region on the hydrogenated and deuterated lipid types with the labeling of deuterated DPPG being on the acyl chain only.

Errors were estimated for model fits where the lipid head and tail groups where treated as separate layers. Individual fit parameters (i.e., layer thickness and SLD) were incrementally adjusted above and below the proposed model fit value until the model to data fit was deemed unsatisfactory. Extremes of each model fit where produced by combining these "unsatisfactory fit parameters" and used to calculate the parameter errors for the proposed models.

Brewster Angle Microscopy. BAM measurements were taken on a BAM2Plus microscope (Nanofilm Technology, Goettingen, Germany) mounted on a Langmuir trough (Model 302m, Nima Technology Ltd., Coventry, UK) equipped with a surface pressure sensor so that the surface pressure and the structure of the surface film could be monitored simultaneously. The microscope was equipped with a frequency doubled Nd:YaG laser (532 nm, 20 mW), polarizer, analyzer, and CCD camera. At the Brewster angle, the reflectivity of *p*-polarized light at the air/water interface is nil; therefore, small changes in the interfacial refractive index, due for example to the presence of a surface film, causes a small amount of the

TABLE 1: Summary of Known Scattering Lengths, Scattering Length Densities, and Molecular Weights of the Lipid and Protein Components Studied

lipid/protein	scattering length (Σb)/10^{-3} Å	scattering length density/10^{-6} Å^{-2}	molecular weight/g mol^{-1}
DPPG headgroup	6.13	2.52	299
h-DPPG	0.39	0.24	721
h-DPPG-tail	−0.32	−0.398	422
d-DPPG	6.84	6.24	783
d-DPPG-tail	0.71	7.54	484
Pin-b	30.7	1.94	12900

p-polarized light to be reflected from the surface. Therefore, a surface film can be visualized by monitoring the intensity of *p*-polarized light over a given area.

Lipid monolayers were created as described for NR studies. Once stable at 22 mN m^{-1}, the protein solution was added to the subphase to reach a final concentration of 0.48 μmol. The surface pressure and structure were then monitored for 260 min after protein addition. BAM images were taken at intervals of 1, 3, 5, 10, 20, 30, 50, 70, 100, 150, 200, and 260 min after introduction of the protein to the aqueous subphase to monitor changes in the lipid monolayer structure. Images were taken using a 10× objective with an actual 15× magnification. This gives an *x*-axis on the image of 430 μm, and the geometry of the *y*-axis was calculated using

$$y = \frac{x}{\alpha \cos \theta} \tag{4}$$

where α is aspect ratio, which is equal to 768/572, and θ is equal to the angle of incidence, which in this case was the Brewster angle of water equal to 53.15°. All experiments were repeated in duplicate.

Results

Characterization of DPPG Monolayer Formation at the Air/Water Interface. Figure 1 shows the surface pressure−area ($\pi-A$) isotherms, BAM images, and NR data for a DPPG monomolecular layer at the air/water interface. During compression of the DPPG layer at the air/water interface, the film underwent phase transitions recorded in the $\pi-A$ isotherms and corresponding changes in domain morphology recorded in BAM images that were consistent with previous work.[28,29] At high area per molecule (>80 Å^2/molecule), the lipid was within a liquid extended or gaseous state and no domain features were observed in the corresponding BAM images. With greater compression, bright polygonal domains evolved in BAM images as regions of concentrated lipid began to form at the interface leading to increased reflection of *p*-polarized light. At low area per molecule (<50 Å^2/molecule), some contrast was evident between lipid domains, which may indicate regions of different average molecular orientation relative to the direction of the incident beam.[29] Altering the polarization resulted in changes to domain contrast suggesting that the observed image contrast was a result of different regions of molecular orientation.

The NR profile of the compressed d-DPPG (chain deuterated) layer held at 22 mN m^{-1} (i.e., within the condensed phase) is shown in Figure 1b. Two fits of the reflectivity profile were performed assuming a single layer and a two layer model. The single layer fit corresponded to a 21 Å lipid layer with a SLD of 5.9 × 10^{-6} Å^{-2} and provided a reasonable fit and definition of the lipid layer. A two layer fit was also performed to differentiate between the deuterated tail region of the lipid and

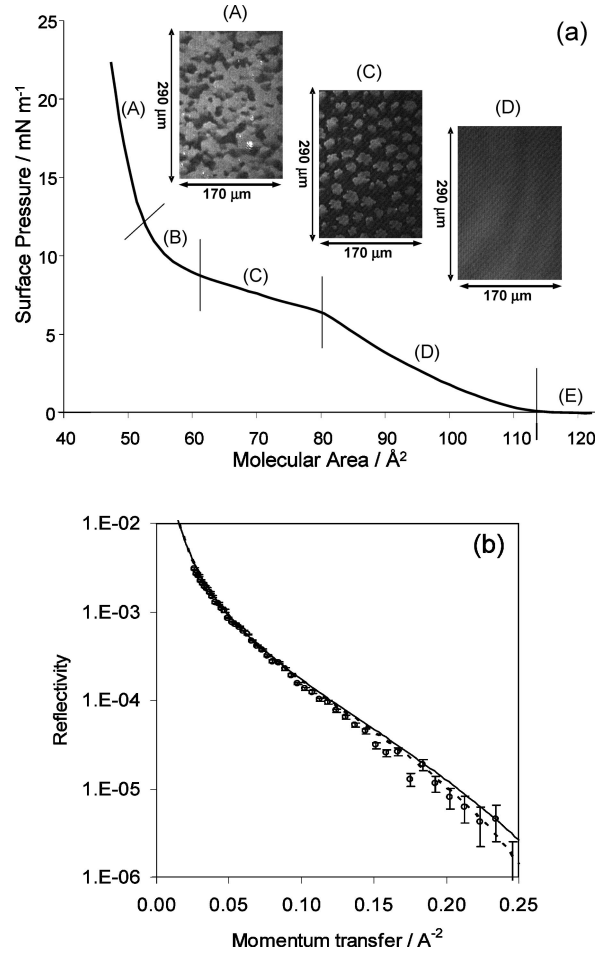

Figure 1. (a) Surface pressure-area ($\pi-A$) isotherm of DPPG showing the five distinct phases of (A) condensed phase, (B) liquid condensed phase, (C) liquid condensed−liquid expanded transition, (D) liquid expanded phase, and (E) liquid expanded-gaseous transition. BAM images show the structure of the lipid monolayer during (A) condensed phase (C) liquid condensed−liquid expanded transition and (D) liquid expanded phase. (b) Neutron reflectivity-momentum transfer plot (after background subtraction) for a compressed DPPG monolayer (○). The dashed line represents the single layer model fit with parameters where $\tau = 21$ Å, $\rho = 5.9 \times 10^{-6}$ Å^{-2}. The solid line represents the two-layer model fit with 1st layer parameters where $\tau = 17$ Å and $\rho = 6.5 \times 10^{-6}$ Å^{-2}, and 2nd layer parameters where $\tau = 6.5$ Å and $\rho = 2.15 \times 10^{-6}$ Å^{-2}.

the hydrogenated head region. This fit was needed for comparison with the protein−lipid data described later, where partial penetration of protein into the lipid region was observed. The solid black line within Figure 1b represents the two layer model fit with first layer parameters corresponding to the hydrophobic tail of $\tau = 17$ Å and $\rho = 6.5 \times 10^{-6}$ Å^{-2} and second layer parameters corresponding to the headgroup of $\tau = 6.5$ Å and $\rho = 2.15 \times 10^{-6}$ Å^{-2}. There was good agreement of total surface excess of lipid between both single and two layer models (2.43 and 2.50 mg m^{-2}, respectively).

Neutron Reflectivity of Pin-b Bound to DPPG Monolayers. Each of the Pin-b proteins was added to a compressed h- or d-DPPG layer and a complete NR profile was recorded after observation that the protein−lipid surface was at or close to equilibrium. The data was fitted using the simplest layer model appropriate to fit both hydrogenated and deuterated contrasts as described in the method section above. The h-DPPG reflectivity profiles could be fitted to a single layer model for each protein; however, this was not possible for the d-DPPG

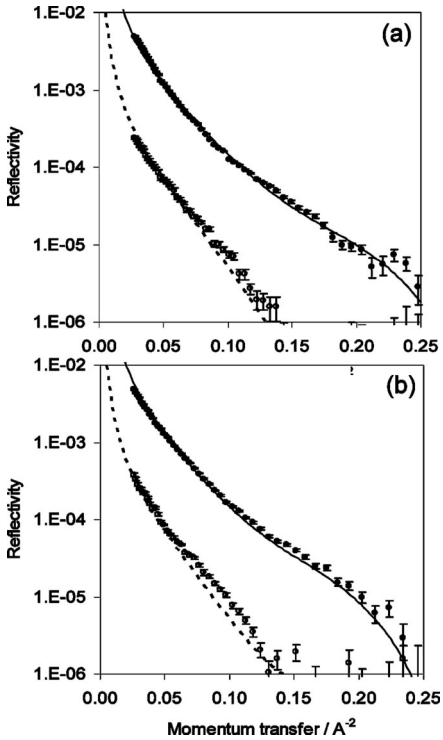

Figure 2. NR profiles (after background subtraction) for (a) Pin-b+ and (b) Pin bS (0.46 μmol) adsorbed to compressed h-DPPG (open circle) and d-DPPG monolayers. For both figures, the solid and dashed lines represent the best two-layer fits to the d- and h-DPPG respectively. For Pin-b+ the model parameters were 1st layer: $\tau = 21$ Å, $\rho_{(h)} = 0.6 \times 10^{-6}$ Å^{-2}, and $\rho_{(d)} = 5.7 \times 10^{-6}$ Å^{-2}; 2nd layer: $\tau = 22$ Å and $\rho = 1.2 \times 10^{-6}$ Å^{-2}.

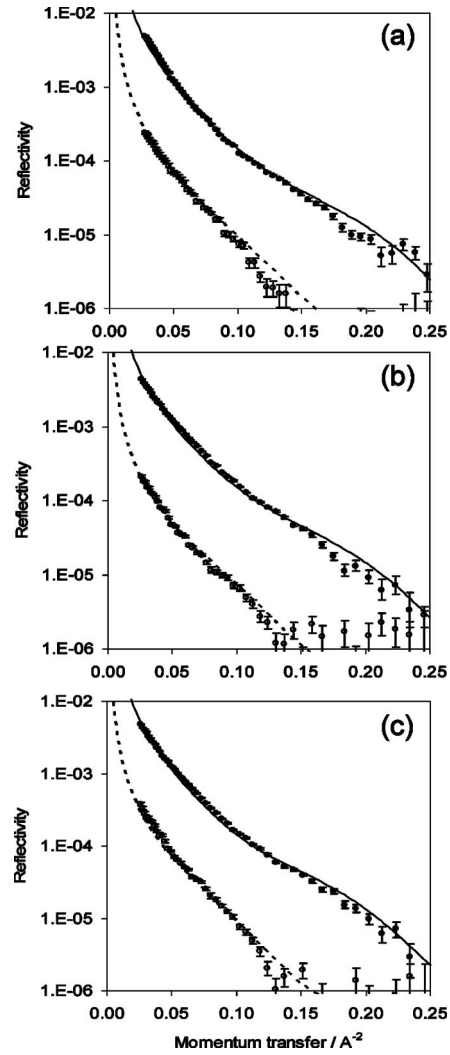

Figure 3. NR profiles (after background subtraction) for (a) Pin-b+, (b) Pin-bH, and (c) Pin bS (0.46 μmol) adsorbed to compressed h-DPPG (open circle) and d-DPPG monolayers. For each figure, the solid and dashed lines represent the best three-layer fits to the d- and h-DPPG, respectively. Model parameters are given in Table 2.

reflectivity profiles. In order to successfully fit both contrasts to a single model, two or three layer fits were required. Using a two layer model it was possible to achieve a satisfactory fit to the experimental NR data for Pin-b+ adsorbed to condensed phase monolayers of h-DPPG and d-DPPG as shown in Figure 2a. This fit for Pin-b+ comprised an upper layer containing 15% protein within a 21 Å thick lipid layer and showed 80% of the total adsorbed protein situated within a second layer below the lipid. Two layer fits for Pin-bS (Figure 2b) and Pin-bH (not shown) were not satisfactory and unable to fully characterize the data for both reflectivity contrasts.

Because of these poor model-to-data fits obtained for Pin-bS and Pin-bH, fits were further refined to enable the lipid region of the interface to be considered as two distinct layers of tail (whether hydrogenated or deuterated) and headgroup. This enabled differences in the extent of penetration of the proteins into the lipid region to be identified. Figure 3 shows the three-layer fits and the NR reflectivity profiles for Pin-b+, Pin-bH and Pin-bS. Since there were just two isotopic contrasts for each protein−lipid system (profiles with hydrogenated and deuterated acyl region of the lipid), fits were carried out by fixing the head and tail of the lipid with the same area per molecule and using this to enable calculation of the amount of protein situated within the head region of the lipid (layer 2). All three-layer fits are summarized in Table 2.

Figure 3a shows the NR profiles and corresponding three-layer fits for the Pin-b+-DPPG system. Pin-b+ was shown to penetrate into the lipid region with 18% of the upper layer made up of protein that had penetrated into the acyl region of the lipid. The three-layer fit showed the acyl region as 17 Å thick in agreement with the lipid only system and also showed a larger proportion of protein (33% of the layer) within the headgroup (charged) region of the lipid, which had increased in thickness from 6.5 to 8 Å on addition of protein. The three-layer model showed that 62% of the total adsorbed protein existed below the lipid region.

For Pin-bH (Figure 3b) and Pin-bS (Figure 3c) the three-layer model provided a satisfactory fit to the data. These fits suggested little penetration of the proteins into the lipid layer with an upper lipid layer consisting of only 5 and 8% Pin-bH and Pin-bS, respectively. However, the three-layer fit revealed that considerable protein was incorporated within the headgroup region of the lipid (35 and 38% of the layer for Pin-bH and Pin-bS, respectively). The three-layer fit revealed that 80 and 75% of the total adsorbed Pin-bH and Pin-bS, respectively, was situated below the lipid region. This was a higher fraction of adsorbed protein than determined for Pin-b+. In addition, the third layer was thicker for both Pin-b mutant forms (26 Å as opposed to 22 Å) than for Pin-b+.

For all three-layer fits to the protein−lipid systems, the lipid region was observed to be consistent with the two-layer model fitted for the lipid-only system (shown in Figure 1b), showing a condensed layer with a volume fraction of 0.84−0.89 lipid in a 17 Å upper acyl layer. The volume fraction dropped from 0.85 to 0.62−0.65 on addition of protein within the charged

TABLE 2: Parameters Obtained from the Best Three-Layer Model Fits of Pin-b Adsorbed to Condensed Phase DPPG Films

contrast + layer	τ/Å	P/10^{-6} Å^{-2}	Γ_{lipid}	$\Gamma_{protein}$	A_{lipid}/Å^2	$A_{protein}$/Å^2	Γ_{lipid}/ mg m^{-2}	$\Gamma_{protein}$/ mg m^{-2}	total $\Gamma_{protein}$/ mg m^{-2}
d-DPPG (1st)	17 ± 1.25	6.5 ± 0.3	0.862 ± 0.04		55.48 ± 6.7		1.52 ± 0.26		
d-DPPG (2nd)	6.5 ± 1	2.15 ± 0.3	0.853 ± 0.08		51.16 ± 11.1		1.52 ± 0.26	0.98 ± 0.24	
Pin-b+									
h-DPPG (1st)	17 ± 0.3	0.01 ± 0.005	0.84 ± 0.01	0.176 ± 0.048	57.21 ± 0.51	5108 ± 1090	1.225 ± 0.01	0.42 ± 0.11	
d-DPPG (1st)	17 ± 0.3	6.65 ± 0.35							
h-DPPG (2nd)	8 ± 0.5	2.4 ± 0.1	0.619 ± 0.05	0.328 ± 0.08	57.21 ± 0.5	5836 ± 1525	0.873 ± 0.01	0.37 ± 0.09	1.95 ± 0.16[a]
d-DPPG (2nd)	8 ± 0.5	2.4 ± 0.1							
h-DPPG (3rd)	22 ± 1	0.8 ± 0.1	0	0.412 ± 0.05	0	1692 ± 184	0	1.27 ± 0.15	
d-DPPG (3rd)	22 ± 1	0.8 ± 0.1							
Pin-bH									
h-DPPG (1st)	17 ± 1	−0.25 ± 0.150.89 ± 0.01	0.053 ± 0.035	53.88 ± 1.42	16929 ± 3482	1.3 ± 0.01	0.184 ± 0.08		
d-DPPG (1st)	17 ± 1	6.8 ± 0.1							
h-DPPG (2nd)	8 ± 1	2.3 ± 0.1	0.64 ± 0.06	0.35 ± 0.08	53.88 ± 0.5	5501 ± 1053	0.91 ± 0.01	0.39 ± 0.01	1.97 ± 0.50[a]
d-DPPG (2nd)	8 ± 1	2.3 ± 0.1							
h-DPPG (3rd)	26 ± 2	0.7 ± 0.001	0	0.52 ± 0.12	0	1354 ± 178	0	1.58 ± 0.18	
d-DPPG (3rd)	26 ± 2	0.7 ± 0.001							
Pin-bS									
h-DPPG (1st)	17 ± 1	−0.2 ± 0.1	0.88 ± 0.01	0.077 ± 0.002	54.26 ± 2.3	11603 ± 2348	1.29 ± 0.1	0.126 ± 0.2	
d-DPPG (1st)	17 ± 1	6.8 ± 0.05							
h-DPPG (2nd)	8 ± 1	2.4 ± 0.1	0.65 ± 0.05	0.38 ± 0.12	54.26 ± 2.3	4943 ± 1540	0.92 ± 0.04	0.43 ± 0.2	1.74 ± 0.09[a]
d-DPPG (2nd)	8 ± 1	2.4 ± 0.1							
h-DPPG (3rd)	26 ± 0.05	0.75 ± 0.05	0	0.36 ± 0.06	0	1527 ± 103	0	1.3 ± 0.2	
d-DPPG (3rd)	26 ± 0.05	0.75 ± 0.05							

[a] Error was estimated for the fitted data by taking extremes of suitable model fits.

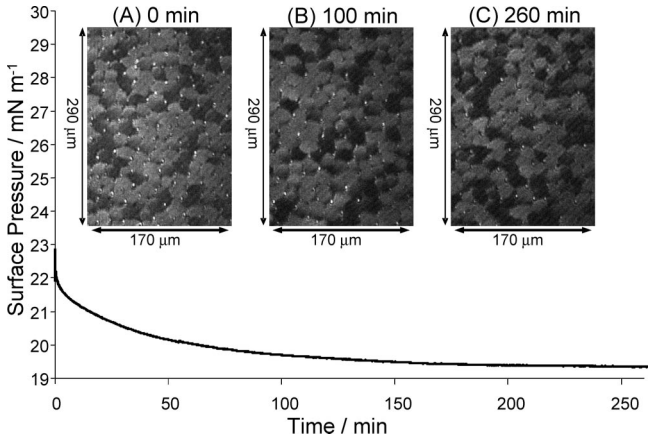

Figure 4. Surface pressure-time isotherms in the presence of a DPPG monolayer compressed to an initial pressure of 22 mN m^{-1} and the corresponding BAM images of the surface taken at 0, 100, and 260 min after the injection of a buffer solution under the lipid film (at 0 min).

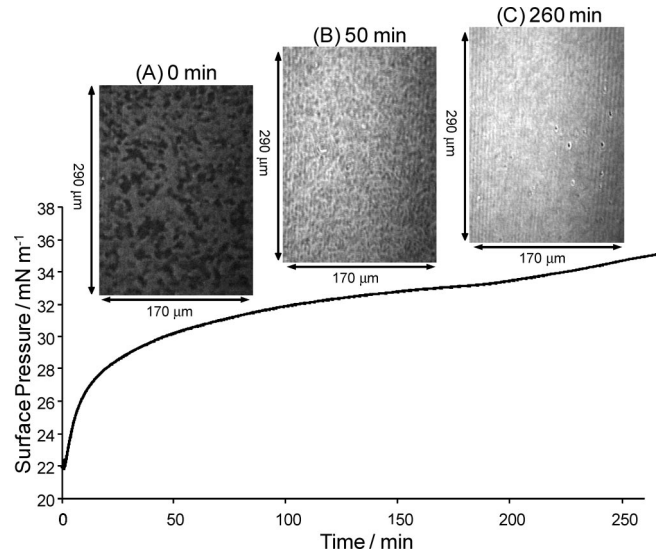

Figure 5. Surface pressure−time isotherms for the interaction of Pin-b+ with a condensed phase monolayer of DPPG and the corresponding BAM images of the surface taken at 0, 50, and 260 min after the injection of the protein under the lipid film.

headgroup layer as its thickness increased to accommodate 33−38% protein.

Brewster Angle Microscopy of Pin-b Bound to DPPG Monolayers. In addition to NR measurements, parallel experiments were performed during which BAM images were taken during adsorption of protein to the DPPG monolayers. These allowed visualization of the changes to the interfacial structure of lipid layers due to penetration and/or adsorption of protein. To allow comparison with our previously published data, surface pressure measurements were recorded simultaneously with BAM images. Figure 4 shows a surface pressure-time profile for a compressed DPPG monolayer with associated BAM images without addition of protein. As seen previously,[17] a small drop in surface pressure is observed over the 4 h time scale of these experiments due to slight reordering of the lipid layer with time. Low levels of impurities in the system may also cause this change. The BAM images across the entire time period appeared to show two visible domain types; these were condensed phase domains with different regions of molecular orientation relative to the incidence beam.[29]

Surface pressure and BAM data for the adsorption of Pin-b+ to DPPG is shown in Figure 5. The surface pressure was seen to increase due to protein adsorption/penetration of the DPPG layer as discussed in our previous work.[17] The corresponding BAM images revealed marked differences from the domain structure seen for the lipid only system. Two changes were observed during adsorption of Pin-b+: first, the overall brightness of the image increased and second, light areas exhibited networked characteristics which became less defined as the image brightness increased. The increase in brightness may have been caused by either the surface film becoming more condensed due to penetration of the protein into the DPPG film, or due to an increase in the thickness of the surface film resulting from protein adsorption below the lipid monolayer.[30] Since the domain structure was seen to change, the increase in brightness was concluded to be at least partly due to the surface lipid layer becoming more condensed as a result of protein penetration.

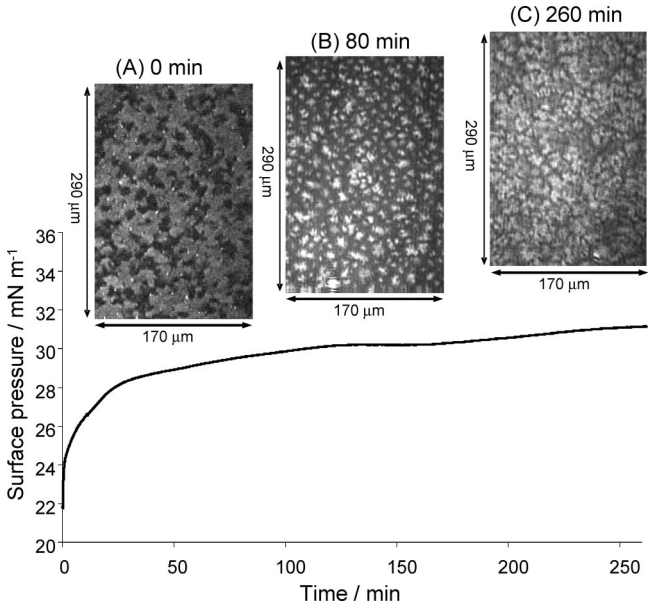

Figure 6. Surface pressure-time isotherms for the interaction of Pin-bH with a condensed phase monolayer of DPPG and the corresponding BAM images of the surface taken at 0, 80, and 260 min after the injection of the protein under the lipid film.

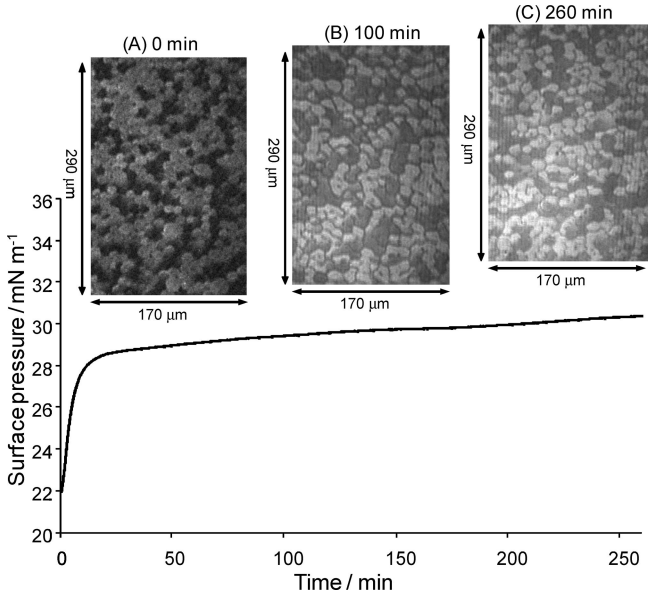

Figure 7. Surface pressure-time isotherms for the interaction of Pin-bS with a condensed phase monolayer of DPPG and the corresponding BAM images of the surface taken at 0, 100, and 260 min after the injection of the protein under the lipid film.

Figure 6 shows the surface pressure-time profile and BAM images for Pin-bH adsorption to DPPG. As seen for Pin-b+, the BAM images increased in brightness indicating an increased layer thickness. In addition, the contrast observed between lipid regions increased, revealing regions of highly condensed lipid (white areas) becoming brighter and larger with time. This provided evidence of lipid rearrangement caused by adsorption and penetration of the protein. Pin-bS BAM images are shown in Figure 7 and reveal a different behavior to both Pin-b+ and Pin-bH. Over a 260 min time period, the domain structure of the lipid remained unchanged in terms of domain dimensions and structure. However, the image increased in brightness as adsorption occurred. Since the lipid domain structure appeared to be unchanged, it can be assumed that changes in the brightness of the image were due to adsorption of protein below the lipid layer and thus an increase in thickness of the interfacial layer. The BAM images showed no evidence of any significant penetration of protein into the lipid layer.

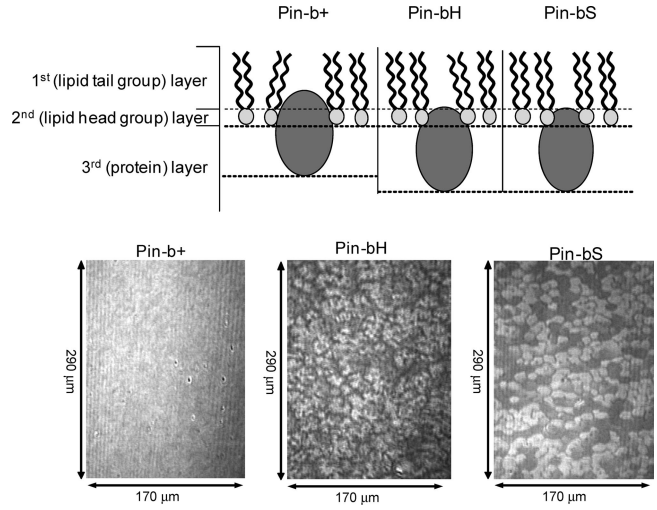

Figure 8. Schematic representation of the difference in penetration of Pin-b+, Pin-bH, and Pin-bS to a condensed phase monolayer of DPPG as suggested by the NR data model parameters proposed in Table 2. Shown also are the final BAM images taken at equilibrium for the corresponding interaction of each puroindoline mutant with a DPPG monolayer.

Discussion

NR profiles for each Pin-b protein adsorbed to DPPG monolayers were fitted using a three-layer model to enable differences in penetration of protein between the lipid headgroup and acyl regions to be determined. The data showed similar adsorbed amounts of each of the three proteins at the interface, with a total surface excess of 1.95, 1.97, and 1.74 mg m^{-2} for Pin-b+, Pin-bH, and Pin-bS, respectively. However, the data also revealed that the depth of penetration of protein into the lipid region differed for each protein, with Pin-b+ penetrating further into the acyl region of the lipid, compared to the mutant forms of the protein that interacted with the headgroup region only. In addition, the protein layer below the lipid region was found to be thicker for the mutant proteins that had penetrated less into the lipid. It is therefore concluded that the differences in lipid binding between Pin-b+, Pin-bH, and Pin-bS are related to their ability to penetrate the acyl chain regions of the anionic DPPG monolayers, as was suggested by our previous surface pressure measurements.[17] The differences in protein binding are shown schematically in Figure 8 with the corresponding final BAM images for each protein.

BAM images were used to characterize the changes in the surface domain structure as a result of Pin-b adsorption to DPPG monolayers and showed some agreement with the NR data for Pin-b+ and Pin-bS adsorbed DPPG films. The domain structure of the condensed phase DPPG monolayer was altered and hardly visible when Pin-b+ adsorption had reached equilibrium, suggesting protein penetration had lead to compression of the lipid region. In contrast the domain structure of the lipid film was unchanged during Pin-bS adsorption to the DPPG monolayer, suggesting no change in compression of the lipid region and little or no penetration of protein into the lipid layer.

Differences in lipid monolayer penetration between Pin-b+ and Pin-bS may derive from the differences in primary structure of the tryptophan-rich loop of each protein with the Pin-bS

mutant containing a W44R substitution within this functional motif. The tryptophan-rich loop of the puroindolines has been suggested to be key to the lipid binding and penetration behavior of the proteins,[31−33] and tryptophan is known to promote the insertion of proteins into lipid aggregates,[32,33] whereas arginine is a highly charged hydrophilic residue. It is therefore probable that Pin-bS binds mainly to the lipid headgroup of the DPPG monolayer due to the increase in hydrophilicity and basicity of the tryptophan-rich loop in this Pin-b mutant. The increase in basic (i.e., cationic) charge would promote electrostatic attractions with the anionic phosphate group on the headgroup of DPPG. This may explain the lower affinity of Pin-bS toward penetration of the acyl chain region of the DPPG monolayer compared to Pin-b+ (with its more hydrophobic tryptophan-rich loop).

The data obtained for Pin-bH appeared to be less conclusive. It was shown by NR that Pin-bH does not penetrate highly into the acyl chain region of the DPPG lipid monolayer, yet the BAM results show that its adsorption caused changes to the domain structures visible at the surface. Pin-bH differs from Pin-b+ by a G46S substitution, again situated within the tryptophan-rich loop of the protein. It has been suggested that the serine residue restricts conformational freedom of the tryptophan-rich loop due to its position within the loop and enables additional H-bonding to further restrict movement.[17] However, the effect the mutation has on the structure of the protein and the loop is unknown at present and can only be postulated. One possiblity that may explain our findings is that the tryptophan-loop of Pin-bH may appear larger and with less conformational freedom than Pin-bS and thus disrupt the headgroup structure in a manner that also effects the acyl chain order without significantly penetrating the acyl region.

Conclusions

The data presented provides structural evidence of the Pin-lipid interface that supports data presented by the authors previously indicating that Pin-b+ is more effective at penetrating DPPG monolayers than either Pin-bH or Pin-bS. This work provides structural evidence that supports our hypothesis that there is a link between the Pin-b lipid binding behavior and the biochemical mechanism that determines wheat endosperm texture. The difference between the lipid binding behavior of the wild type versus the mutant forms of Pin-b also could have an impact on their antimicrobial behavior and may be linked to a weakening of seed defense in hard wheat varieties.

Acknowledgment. This work was supported by the U.K. Biotechnology and Biological Sciences Research Council (Studentship BBSSA200411018) and by ISIS Beamtime Awards RB520282 and RB620480 from the Science and Technology Facilities Council. We thank Campden & Chorleywood Food Research Association for the donation of wheat flour samples.

References and Notes

(1) Blochet, J.-E.; Chevalier, C.; Forest, E.; Pebay-Peyroula, E.; Gautier, M.-F.; Joudrier, P.; Pezolet, M.; Marion, D. *FEBS Lett.* **1993**, *329*, 336.

(2) Gautier, M.-F.; Aleman, M. E.; Guiro, A.; Marion, D.; Joudrier, P. *Plant Mol. Biol.* **1994**, *25*, 43.

(3) Dubreil, L.; Vie, V.; Beaufils, S.; Marion, D.; Renault, A. *Biophys. J.* **2003**, *85*, 2650.

(4) Dubriel, L.; Compoint, J. P.; Marion, D. *J. Agric. Food Chem.* **1997**, *45*, 108.

(5) Greenblatt, G. A.; Bettge, A. D.; Morris, C. F. *Cereal Chem.* **1995**, *72*, 172.

(6) Greenwell, P.; Brock, C. J. *Cereal Foods World* **1993**, *38*, 615.

(7) Jolly, C. J.; Rahman, S.; Kortt, A. A.; Higgins, T. J. V. *Theor. Appl. Genet.* **1993**, *86*, 589.

(8) Krishnamurthy, K.; Balconi, C.; Sherwood, J. E.; Giroux, M. J. *Mol. Plant-Microbe Interact.* **2001**, *14*, 1255.

(9) Charnet, P.; Molle, G.; Marion, D.; Rousset, M.; Lullien-Pellerin, V. *Biophys. J.* **2003**, *84*, 2416.

(10) Faize, M.; Sourice, S.; Dupuis, F.; Parisi, L.; Gautier, M.-F.; Chevreau, E. *Plant Sci.* **2004**, *167*, 347.

(11) Mattern, P. J.; Morris, R.; Schmidt, J. W.; Johnson, V. A. *Location of the Genes for Kernal Properties in the Wheat Cultivar "Cheyenne" using Chromosome Substitution Lines*, Proceedings of the 4th International Wheat Genetics Symposium, Columbia, MO, 1973; Sears, E. R., Sears, L. M. S., Eds.; University of Missouri Press: Columbia, MO, 1973; 703.

(12) Sourdille, P.; Perretant, M. R.; Charmet, G.; Leroy, P.; Gautier, M. F.; Joudrier, P.; Nelson, J. C.; Sorrells, M. E.; Bernard, M. *Theor. Appl. Genet.* **1996**, *93*, 580.

(13) Giroux, M. J.; Morris, C. F. *Theor. Appl. Genet.* **1997**, *95*, 857.

(14) Giroux, M. J.; Talbert, L. E.; Habernicht, D. K.; Lanning, S.; Hemphill, A.; Martin, J. M. *Crop Sci.* **2000**, *40*, 370.

(15) Beecher, B.; Bettge, A.; Smidansky, E.; Giroux, M. J. *Theor. Appl. Genet.* **2002**, *105*, 870.

(16) Clifton, L. A.; Green, R. J.; Frazier, R. A. *Biochemistry* **2007**, *46*, 13929.

(17) Clifton, L. A.; Lad, M. D.; Green, R. J.; Frazier, R. A. *Biochemistry* **2007**, *46*, 2260.

(18) Lad, M. D.; Birembaut, F.; Clifton, L. A.; Frazier, R. A.; Webster, J. R. P.; Green, R. J. *Biophys. J.* **2007**, *92*, 3575.

(19) Green, R. J.; Su, T. J.; Lu, J. R.; Webster, J. R. P. *J. Phys. Chem. B* **2001**, *105*, 9331.

(20) Wu, F.; Gericke, A.; Flach, C. R.; Seaton, B. A.; Mendelsohn, R. *Biophys. J.* **1998**, *74*, 306.

(21) Mowald, H. *Rep. Prog. Phys.* **1993**, *56*, 653.

(22) Penfold, J.; Richardson, R. M.; Zarbakhsh, A.; Webster, J. R. P.; Bucknall, D. G.; Rennie, A. R.; Jones, R. A. L.; Cosgrove, T.; Thomas, R. K.; Higgins, J. S.; Fletcher, P. D. I.; Dickinson, E.; Roser, S. J.; McLure, I. A.; Hillman, A. R.; Richards, R. W.; Staples, E. J.; Burgess, A. N.; Simister, E. A.; White, J. W. *J. Chem. Soc., Faraday Trans.* **1997**, *93*, 3899.

(23) Green, R. J.; Su, T. J.; Lu, J. R.; Penfold, J. *J. Phys. Chem. B* **2001**, *105*, 1594.

(24) Green, R. J.; Su, T. J.; Lu, J. R.; Webster, J.; Penfold, J. *Phys. Chem. Chem. Phys.* **2000**, *2*, 5222.

(25) Green, R. J.; Su, T. J.; Joy, H.; Lu, J. R. *Langmuir* **2000**, *16*, 5797.

(26) Born, M.; Wolf, E. *Principles of Optics*; Pergamon Press: Oxford, 1970.

(27) Penfold, J. *Curr. Opin. Colloid Interface Sci.* **2002**, *7*, 139.

(28) Minones, J.; Rodriguez-Patino, J. M.; Minones, J.; Dynarowicz-Latka, P.; Carrera, C. *J. Colloid Interface Sci.* **2002**, *249*, 388.

(29) Minones, J.; Dynarowicz-Latka, P.; Minones, J.; Rodriguez-Patino, J. M.; Iribarnegaray, E. *J. Colloid Interface Sci.* **2003**, *265*, 380.

(30) Cejudo-Fernandez, M.; Carrera-Sanchez, C.; Rodriguez-Nino, M. R.; Rodriguez-Patino, J. M. *Langmuir* **2007**, *23*, 7178.

(31) Kooijman, M.; Orsel, R.; Hamer, R. J.; Bekkers, A. C. A. P. A. *J. Cereal Sci.* **1998**, *28*, 43.

(32) Yau, W. M.; Wimley, W. C.; Gawrisch, K.; White, S. H. *Biochemistry* **1998**, *37*, 14713.

(33) Petersen, F. N. R.; Jensen, M. O.; Nielsen, C. H. *Biophys. J.* **2005**, *89*, 3985.

JP806016H